ADVANCED FUNCTIONAL MATERIALS
www.afm-journal.de

Materials Views
www.MaterialsViews.com

# Self-Organization and/or Nanocrystallinity of Co Nanocrystals Effects on the Oxidation Process Using High-Energy Electron Beam

*Ana Cazacu, Claudio Larosa, Patricia Beaunier, Guillaume Laurent, Paolo Nanni, Liliana Mitoseriu, and Isabelle Lisiecki**

**The enhanced stability of Co nanocrystals (NCs) when they are highly ordered at both nanometer and micrometer scales is reported. For the first time, it is shown that both the crystalline structure of Co nanoparticles (NPs) and their 2D hexagonal organization have a significant impact on the oxidation process rate enabling to produce various types of nanostructures including core-shell NPs. The Co core can be either polycrystalline or hexagonal close-packed (hcp) single-crystalline, whereas the oxide shell is composed either of CoO or of the spinel structrure $Co_3O_4$. The present results are evidenced through a careful high-resolution transmission electron microscopy (HRTEM) study and are highly reproducible.**

## 1. Introduction

Inorganic nanoparticles (NPs) with well-defined structural characteristics (composition, size, geometry, and crystalline structure) have attracted a great deal of attention not only for their fundamental interest, but also for the applicative possibilities in fields such as catalysis, energy storage and conversion and information technology.[1–8] When they are characterized by a narrow size distribution, they can be used as building blocks in two- and three-dimensional superlattices,[9–15] whose unique properties are determined not only by the atomic structure, but also by the interparticle interaction. Thus, in recent years, specific mechanical,[16] transport,[17] magnetic,[18–20] optical,[21–24] vibrational,[25–27] and chemical[28–34] properties have been shown to arise from long-range mesoscopic organization of nanocrystals (NCs). However, the influence of the NP crystalline structure (also called nanocrystallinity) on the physical and chemical properties has been scarcely studied.[30–35] This is clearly due to the difficulties encountered by the researchers in controlling nanocrystallinity while, all the other parameters are kept unchanged (composition, size, geometry, stability, and coating agent). Using our ability to control both Co nanocrystallinity and NP organization, we showed very recently, a metallic structure effect on the nano-Kirkendall process occuring only when NCs are closely packed in a 2D array.[30] Although transmission electron microscopy (TEM) is a powerful technique for the observation of NP structures, it is also well known to induce structural and chemical transformations.[36–41] In this paper, we have used an electron beam not only to characterize Co NCs but also as a tool in order to study their stability as a function of their mesoscopic organization and their crystalline structure. Our results show that cobalt NCs, when exposed to a high-energy and controlled electron beam, can partially oxidize, forming Co-core/Co-oxide shell structures. Co NC oxidation is found to be greatly hindered if they are single-crystalline and/or closely packed in a hexagonal network. We show for the first time that the kinetic transformation rate depends on both the particle nanocrystallinity and/or their structural environment. We are able to control both the structural Co core, which can be polycrystalline or hexagonal close-packed (hcp) single-crystalline and the nature of the Co-oxide (either CoO or $Co_3O_4$). We emphasize that, in addition to the fundamental aspect of this study, the control and/or prediction of the nature of the Co-oxide growing at the surface of the Co core is an important topic for many potential applications. For example, the monoxide is highly desirable for high-density magnetic storage,[8] whereas the spinel oxides are expected to be ideal candidate materials for Li-ion batteries.[7]

Dr. A. Cazacu, Dr. C. Larosa, Dr. P. Nanni
Department of Chemical and Processing Engineering
University of Genoa
via Balbi, 5, 16126, Italy
Dr. A. Cazacu, Prof. L. Mitoseriu
Department of Physics
"Al. I. Cuza" University of Iasi
Carol I Blvd., 11A, 700506, Romania
Dr. P. Baunier
UPMC, Univ Paris 06
UMR 7197, LRS, Le Raphaël
3 rue Galilée, 94200 Ivry, France
Dr. G. Laurent, Dr. I. Lisiecki
CNRS, Univ Paris 06
UMR 7070, LM2N, bât. F, B.P. 52, 4 place Jussieu
Paris F-75231 Cedex 05,France
E-mail: isabelle.lisiecki@upmc.fr

**DOI: 10.1002/adfm.201301465**

## 2. Results

For this study, some drops of a colloidal solution of Co NCs dispersed in hexane, were deposited on amorphous carbon-coated copper grid, suitable for TEM observations. The dodecanoic acid-coated Co NCs are either poorly crystallized (polycrystals) or hcp single crystals, and can be either isolated or self-organized in 2D arrays. The images were recorded at intervals of 1 min up to a maximum of 19 min (see Experimental Section for further explanations).

We performed a comparative study of the resistance under electron beam irradiation of Co nanocrystals as a function of both their organization on the substrate (**Figure 1**) and the Co nanocrystalinity (**Figure 2**). First, we focused on the polycrystal organization effect under irradiation. Co polycrystals obtained just after synthesis are characterized by a mean size and size distribution of 7.1 ± 0.4 nm and 9.5% (Figure 1A).[43] HRTEM image (**Figure 3**C) displays few crystalline domains, whose typical size does not exceed 1 nm, indicating a highly disordered polycrystalline structure that is further confirmed by a wide diffuse ring in the corresponding power spectrum (Figure 3A). Figure 1A shows a TEM image of a 2D hexagonal array of Co polycrystals coexisting with the isolated ones. The mean interparticle distance in the 2D array is 2 nm (Figures 1A,2A). Whatever the particle environment, the mean particle size remains unchanged and the particle contours appear always well defined, without core-shell contrast, suggesting the absence of oxidation. We studied the effects of irradiation exposure using a magnification of 250 000 times with an electron beam spread to obtain a low electron current density. After 5 min, the TEM study reveals that isolated NCs start to be surrounded by diffuse intensity, which suggests the presence of shell-like structure that progressively expands at the expense of the core, with increasing irradiation time. At 15 min, Figure 1B clearly shows that Co NCs, when self-organized, remain almost unchanged whereas the isolated ones have undergone a drastic structural transformation from uniform 7.1 nm-NCs to core-shell structures. The residual core and expanded shell are found equal to 4.4 nm and 3.9 nm respectively, giving a total diameter of around 12.2 nm. The HRTEM image shown in Figure 1C (selected area of Figure 1B) reveals that the shell is composed of crystallized domains characterized by three sets of lattice planes. The characteristic distances, accurately measured on the power spectrum (Figure 1D) are found equal to 2.00 Å, 2.41 Å, and 2.88 Å, corresponding to the (400), (311), and (220) planes of $Co_3O_4$ phase respectively. Therefore, while self-organized Co polycrystals remain stable, the isolated ones have already transformed into core (Co)-shell ($Co_3O_4$) NCs. This study clearly demonstrates that the 2D organization induces greater stability against such oxidation compared to the same NCs when isolated.

A second set of experiments was dedicated to a comparative study of the enhanced stability of the 2D organizations composed of either poorly crystallized Co NCs or hcp-Co single crystals. Hcp-Co single crystals were obtained by solution-phase annealing of the Co polycrystals.[44] The HRTEM images show one single NP characterized by two sets of lattice planes with 2.01 Å and 2.18 Å spacing corresponding to the (002) and (100) planes of Co-hcp structure (Figures 2F,3E,G). The average diameter of the single crystals is slightly decreased by comparison to one of the polycrystals, that is, 6.8 nm against 7.1 nm while the size distribution remains constant, of 9.4%. Similarly to the polycrystals, the single-crystals self-organize into a 2D hexagonal array with an interparticle gap distance of 2 nm (Figure 2F). We studied the structural changes for both polycrystalline and single-crystalline samples. Using a magnification of 800 000 times, the electron beam was focused on the sample in order to conserve the same current density as in previous experiments (5.7 pA $cm^{-2}$). Let us first focus on the polycrystalline sample. For the first 5 min, Co NCs do not undergo any structural transition (Figures 2A,B,3A,C). They remain poorly crystallized and no trace of oxide can be detected. Conversely, at 6 min, a few lattice planes with 2.46 Å and 2.1 Å distances start to develop and correspond, without any ambiguity, to the (111) and (200) lattice planes of CoO (Figure 2C and selected area). By increasing the exposure time to 10 min, CoO domains progressively growth, giving rise to structures that we entitle as "scales" (Figure 2D and selected area). These domains remain unchanged until 16 min, when they suddenly transform into the spinel structure $Co_3O_4$. This transition is well illustrated by the HRTEM images (Figures 2E,3D) and corresponding power spectra (Figure 3B), which show new distances, that is, 2.32 Å and 2.02 Å related to (222) and (400) lattices planes of the spinel oxide, respectively. It is worth to underline that the oxidation induced by high-energy electron beam exposure for 16 min is not accompanied neither by aggregation nor by coalescence between NCs, which remain well organized in a 2D array with unchanged hexagonal parameter. By subjecting the 2D arrays composed of hcp single crystals to rigorously the same irradiation treatment employed for the polycrystalline sample (Figure 2G–J), no structural change is noticed. The 2D organizations keep their integrity (Figure 2J) and the three sets of lattice planes characterized by 1.91 Å, 2.01 Å, and 2.17 Å spacings corresponding to the (101), (002), and (100) lattice planes, well indicate the presence of pure hcp Co (Figure 3F,H). Whatever the nanocrystallinity, we observe that

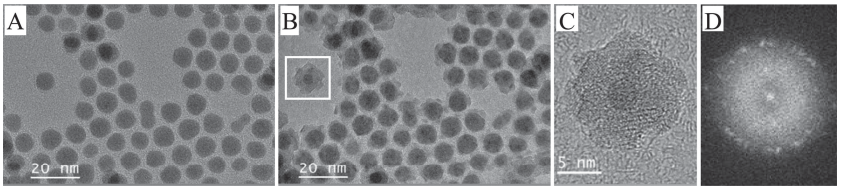


**Figure 1.** HRTEM images of Co polycrystals after exposure to electron beam irradiation for: A) 0 min, B) 15 min, C) selected area of (B) at 16.5 min. D) The power spectrum of (C).

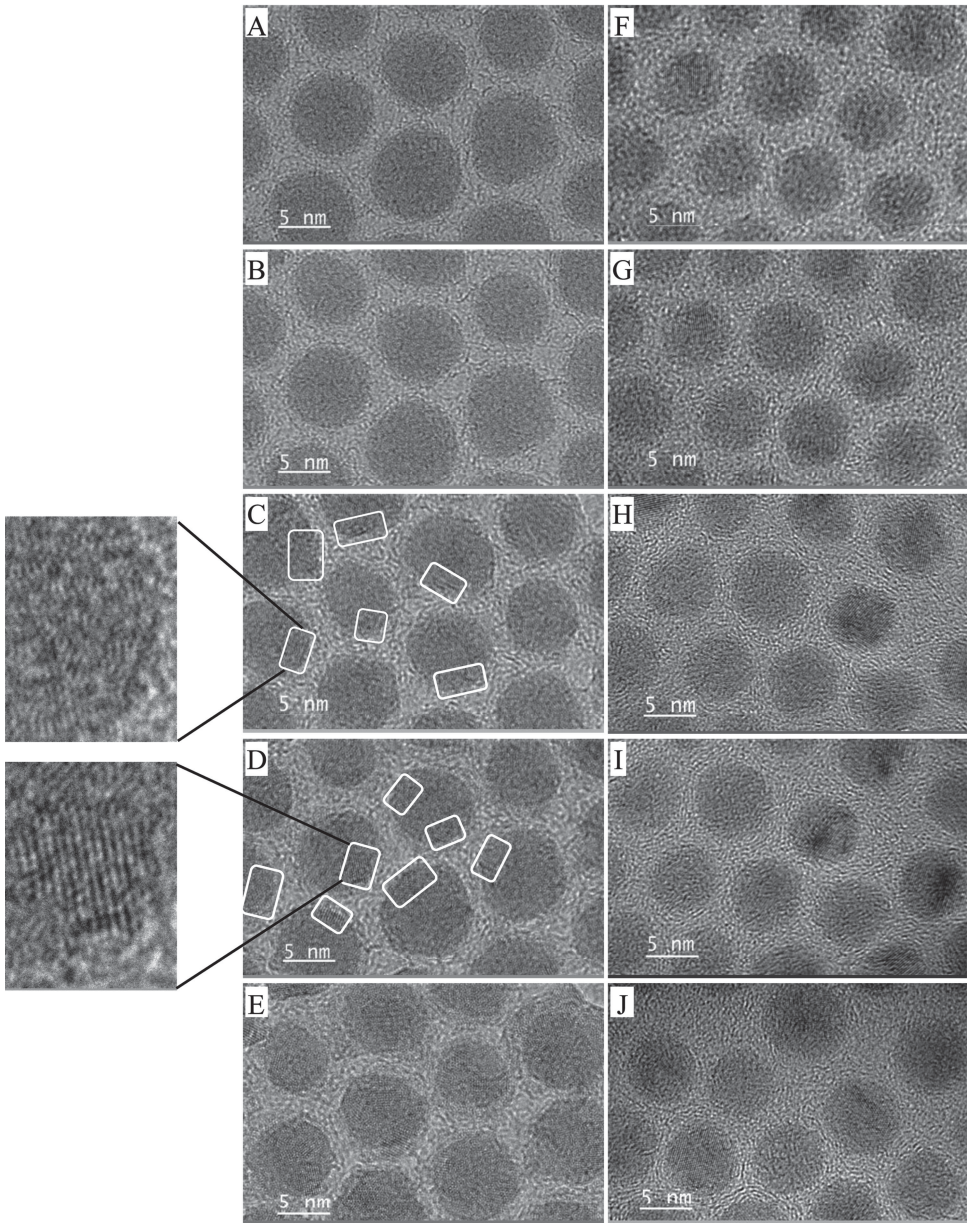


**Figure 2.** HRTEM images of Co polycrystals under electron beam irradiation for: A) 0 min, B) 1.5 min, C) 6 min, D) 10 min, E) 16 min; and of hcp-Co single-crystals for F) 0 min, G) 5 min, H) 7 min, I) 10 min, and J) 16 min.

particle size never changes. Further irradiation left the two systems unchanged. This result demonstrates that Co NCs closed packed in a hexagonal array are much more robust and stable under high-energy electron beam when they are highly crystallized in a hcp structure.

To determine the extend of Co nanocrystallinity effect on the NP stability, we performed a last series of experiments involving isolated Co NCs (Figures 2,3). **Figure 4** illustrates the various behaviors observed after irradiation times of up to 15 min for poorly crystallized Co polycrystals and hcp-Co NPs, characterized by similar initial mean diameter, that is, 6.6 nm and 6.4 nm respectively (Figure 4A,G). Starting from 2.5 min, the HRTEM image of the polycrystal (Figure 4C) already reveals structural changes (Figure 4A,B). The NC is surrounded by diffuse intensity, which suggests the presence of a core/shell structure. Besides, an extra growth domain appears at one particle edge (Figure 4C, selected area), showing lattice planes with 2.38 Å and 2.4 Å distances corresponding to the (222) and (311) planes of $Co_3O_4$. The mean core diameter and shell thickness are found equal to 6.3 nm and 1.33 nm respectively, giving a mean NC diameter of 8.9 nm, against 6.6 nm for the initial NC. By further irradiating the particle, the core size drastically decreases, whereas the shell expands (Figure 4D–F). At 6.5 min and 15 min (Figure 4E,F), lattice

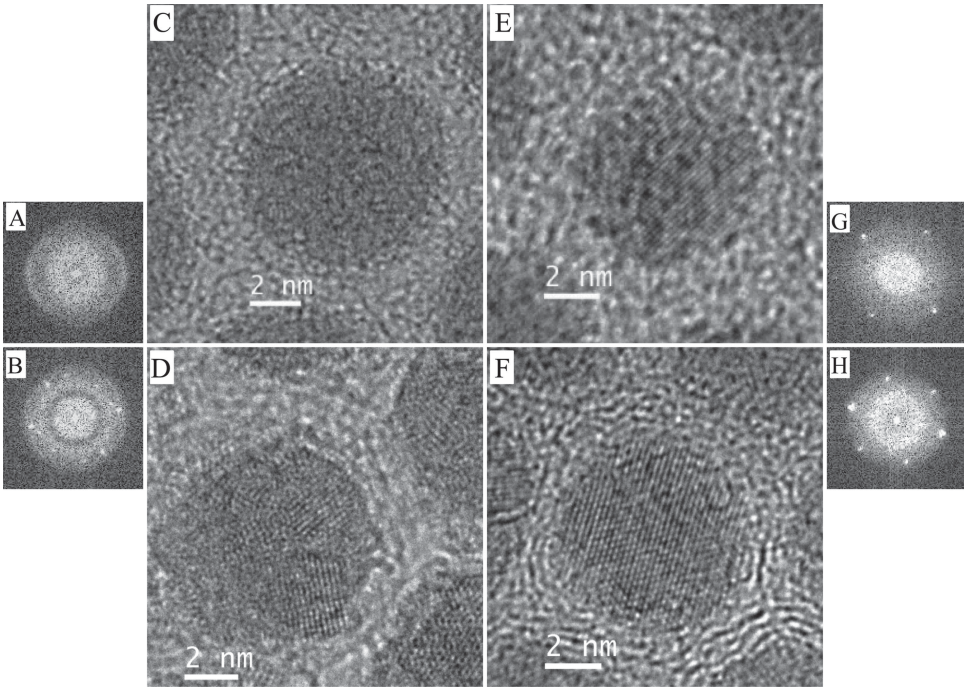


**Figure 3.** Power spectra and HRTEM images of a Co polycrystal: A,C) after 0 min and B,D) 16 min of irradiation; and an hcp-Co single-crystal: E,G) after 0 min and F,H) 16 min of irradiation. NCs are selected from the Figure 2.

planes are well visible all over the particle with an additional distance equal to 2.8 Å, corresponding to (220) spacing of $Co_3O_4$. This feature further confirms the presence of a pure spinel structure. After 15 min, the induced core-shell structure is characterized by mean sizes of the core and shell equal to 3 nm and 3.75 nm respectively. From this result, we conclude that the 10.5 nm NC is composed of a poorly crystallized Co core and a highly crystallized $Co_3O_4$ shell. The same treatment performed on the hcp single crystals produces a rather different behavior. One example is illustrated through the HRTEM images in Figure 4G–M. Conversely to the polycrystalline case, no change occurs before 5 min (Figure 4G,I). At 5 min, a domain initiates at one edge of the particle (Figure 4J, selected area) showing lattice planes with 2.13 Å distance corresponding to the (200) planes of CoO. Further increase in the irradiation time results in the growth of this oxide domain while new ones initiate (Figure 4K). Domain size progressively increases, and at 8.6 min (Figure 4l), (220) planes of $Co_3O_4$ can be identified. At 15 min, 8.3 nm-NCs are characterized by a core-shell structure with a mean core diameter and shell thickness equal to 5.6 nm and 1.33 nm respectively. The coexistence of 2.13 Å and 2.8 Å distances indicates the presence of both (200) planes of CoO and (220) planes of $Co_3O_4$ in the shell, while the core probably keeps the hcp structure. In conclusion, the significant time increase observed for the structural change occurring under electron beam between the two crystallographic structures combined with different oxidation processes denote a significantly enhanced stability of Co-hcp single crystals by comparison to the poorly crystallized NPs.

### 2.1. Discussion

Our results show that Co NCs are more stable under a high-energy electron beam if they are self-organized in a 2D hexagonal array and highly crystallized into hcp single crystals. However, when transformations occur, they clearly result in the oxidation of the metal into either CoO or $Co_3O_4$. This rather unexpected behavior is explained by the combination of a local-scale elevated temperature and the presence of oxygen. Despite the fact that the synthesis and preparation of the 2D superlattices were carried out in an $N_2$ glove box, residual oxygen remains trapped in the amorphous carbon of the TEM grid.[36] High local temperature combined with quite high vacuum ($2 \times 10^{-5}$ Pa) favors the release of oxygen from the carbon film. Hence, $O_2$ molecules can diffuse through the organic shell on the Co NCs by direct interchange of Co and O atoms, inducing metal oxidation.

Whatever the cobalt nanocrystallinity, we have shown that the oxidation process is hampered when the NCs are organized in a hexagonal array, by comparison to the isolated NCs. This change of stability as a function of self-organization on the substrate is partly explained by a change in the permeability of dodecanoic acid chains to oxygen.[46] In a 2D array, the alkyl chains, covalently bonded to Co surface, are confined to the spaces between the NCs and either interdigitate with neighboring NCs or form a continuous shell.[43,47,48] Compared to the single layer surrounding an isolated NC, the diffusivity of oxygen atoms is significantly reduced and this inhibits the oxidation of NCs.[46] On the other hand, a change in the red-ox potential of the $Co/O_2$ couple with the structural environment

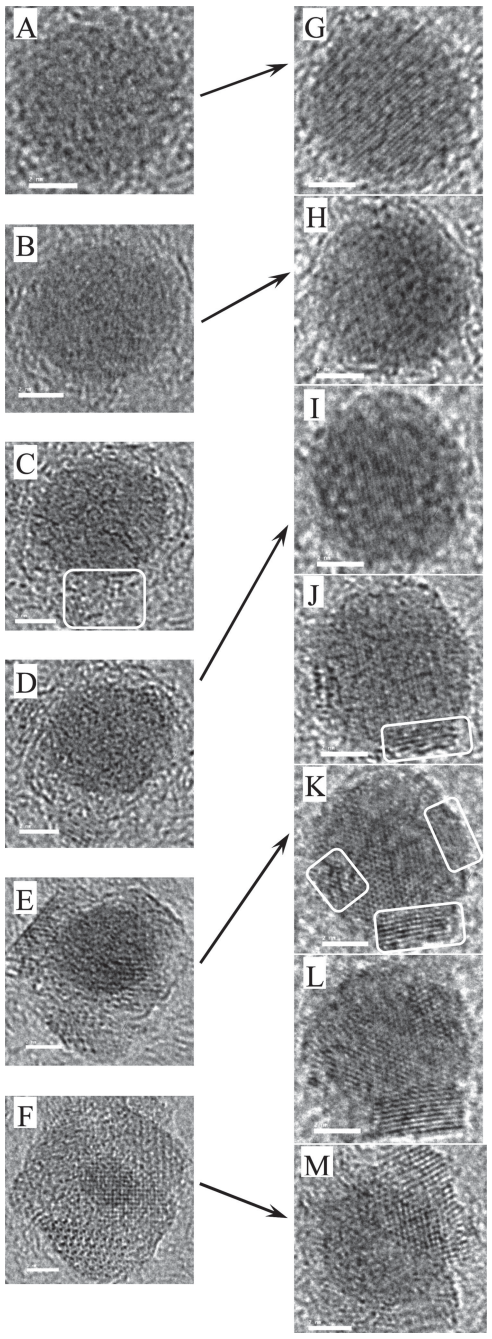


**Figure 4.** HRTEM images of an isolated polycrystal after electron beam exposure for: A) 0 min, B) 1.5 min, C) 2.5 min, D) 3.5 min, E) 6.5 min, F) 15 min; and of an isolated hcp single-crystal for: G) 0 min, H) 1.5 min, I) 3.5 min, J) 5 min, K) 5.6 min, L) 8.6 min, M) 15 min. Scale bars represent 2 nm. The arrows indicate the images taken at the same electron beam exposure.

of Co NCs cannot be excluded and such effect could contribute to their higher resistance to oxidation when they are close packed in a 2D array. This result reinforces the role played by the 2D self-organizations of metallic NPs on their chemical stability properties.[29,36] It is also consistent with the large effective Young's modulus found on 2D arrays of dodecanethiol-ligated 6 nm-Au NCs, which indicates a high tensile strength that has been attributed to the strong interaction between coating molecules in the vicinity of the NCs.[49] Finally, as well illustrated in the HRTEM images (Figures 2J,3F), the significant increase in the contrast of the area surrounding the NCs with increasing the exposure time, is probably related to the graphitization of the coating chains, which results in the formation of a highly protective shell.[50] While the stability of the 2D arrays is mainly ensured at low exposure time by the self-organization effect, it is probably reinforced at higher exposure time by the alkyl chain graphitization.

Using our ability to control accurately the nanocrystallinity of Co NPs (while keeping unchanged their size, and coating agent) from highly disordered polycrystals to hcp single crystals, we highlight an unambiguous nanocrystallinity effect on the electron beam-induced oxidation. The higher the Co nanocrystallinity, the higher the NP robustness. Co polycrystals are composed of crystallized domains with sizes below 1 nm, and contain numerous defects, such as grain boundaries, whereas single crystals are totally defect-free. Within the poorly crystallized NPs, it is likely that the diffusion process, via direct interchange of Co and O atoms, preferentially occurs along the defects and not along the hcp lattice planes, as this is the only possibility within the single crystals. The oxidation is then more favorable in polycrystals than in single crystals. Here too, a change in the red-ox potential of the $Co/O_2$ couple with the nanocrystallinity of Co NCs could contribute to their higher resistance to oxidation when they are highly ordered.

To the best of our knowledge, in the literature, the nanocrystallinity has been rarely taken into account in the understanding of the physico-chemical properties of such particles. The lack of results in this domain is mainly related to the difficulty of accurately controlling this parameter while keeping unchanged the other structural characteristics (size, shape, and coating agent). Some reports relate the nano-Kirkendall effect to the crystalline structure of silver NCs.[32] Recently, we have shown the very low effect of the nanocrystallinity of the same Co NPs on the acoustic breathing mode frequency,[33] while a total absence of structural characteristic effect is observed during the oxidation under oxygen of the same Co NCs isolated on the substrate.[30] Here, we have shown that isolated Co-hcp single crystals are much more stable under a high-energy electron beam than poorly Co crystallized polycrystals resisting oxidation for longer. In addition, the oxides formed are $Co_3O_4$ in the first case and CoO in the second one. For the first time, we have clearly demonstrated the significant impact of crystallographic nanostructure on the oxidation process of isolated Co NCs. We emphasize that Co NCs studied here are characterized by the same size, shape and coating agent, whatever their nanocrystallinity.

This study permits to conclude that Co NCs are significantly more robust under a high-energy electron beam when they are: 1) highly crystallized and 2) closely packed in a 2D hexagonal network. In addition, the more stable systems, when they undergo oxidation, always transform from Co to CoO, while the less stable systems directly oxidize in the spinel form $Co_3O_4$. Actually, $Co_3O_4$ is the most thermodynamically stable form of cobalt oxide, but requires relatively high temperatures to form.[51] The difference in the nature of the oxide we obtain is explained by the stability effect of the Co NPs. The higher

the NC stability, the slower the kinetic formation of the Co-oxide, thus favoring CoO formation. Conversely, the use of a less stable system (isolated polycrystals) drives faster the kinetic formation of the oxide, preventing the transition to CoO to give rise directly to $Co_3O_4$. The oxidation behaviors reported here have been reproducible several times with two different TEM apparatus.

Finally, such an in-situ study meets together an efficient way to oxidize the sample and a powerful tool to simultaneously characterize the induced-structural transformation. It is highly important to notice that these specific conditions (particular apparatus, vapor pressure of oxygen, diameter of the beam, etc.) allowed us to accurately evidence the nano- and super-crystallinity effects on the oxidation process, which would be more ambiguous otherwise. Even if the oxidation conditions are specific to TEM experiments, the obtained results are, nevertheless, characteristic to the NPs oxidation behaviour and thus constitute a good predictive model. This investigation could be extended to other oxidizible nanomaterials in order to provide additional informations on the impact of the structural characteristics on the oxidation of materials based on NCs, that suffer, even today, of a severe lack of knowledge.

## 3. Conclusions

Our results clearly show the effects of nanocrystallinity and/or self-organization of Co NPs on their stability under a high-energy electron beam. For the first time, we have shown that the irradiation-induced oxidation rate drastically depends on these two structural parameters. Hcp-Co single crystals self-organized in 2D hexagonal arrays never oxidize, whereas poorly crystallized Co polycrystals, isolated on the substrate, tend to rapidly oxidize into core (Co)-shell ($Co_3O_4$) structure. As a result of the interdependence between the NP stability and the kinetic oxidation rate, the obtained oxide shell can be either CoO or $Co_3O_4$.

## 4. Experimental Section

*Products*: All materials were used without further purification: cobalt acetate, dodecanoic acid, sodium borohydride, and octylether are from Aldrich, isooctane and hexane from Fluka, sodium di(ethylhexyl) sulfosuccinate (NaAOT) from Sigma. The synthesis of cobalt (II) bis(2-ethylhexyl) sulfosuccinate ($Co(AOT)_2$) was described previously.[42]

*Apparatus*: High-resolution transmission electron microscopy was performed using a JEOL JEM 2010 UHR microscope equipped with an $LaB_6$ filament and operating at 200 kV. The images were collected with a 4008 × 2672 pixel CCD camera (Gatan Orius SC1000) coupled with the DIGITAL MICROGRAPH software. For all the studies, images were recorded at intervals of about every 1 min up to a maximum of 19 min in order to see the evolution of Co NCs under the electron beam exposure. A typical capture time is 1 s for each image to limit the electron beam effect. Two magnifications of the images were chosen to observe the phenomena.

*Synthesis of Co Polycrystals*: Co NCs stabilized by dodecanoic acid chains are synthesized via chemical reduction in reverse micelles (water in oil droplets) as described in a previous paper.[43] By controlling the reducing agent (sodium borohydride) concentration, a narrow size distribution of Co NCs is obtained. The NCs are dispersed in hexane.

*Synthesis of Hcp-Co Single Crystals*: Octylether, having the boiling point at 286 °C, was used as solvent in order to anneal the native Co NCs at 250 °C. Thus, 2 mL of $10^{-2}$ M Co NCs colloidal solution were evaporated to remove the hexane and after that, the resulting powder was redispersed in octylether (5 mL).[44,45]

A refluxing bath, consisting of a four-necked flask, was used for the annealing treatment. This permits the use of a nitrogen flux, control of the solution temperature, solution injection and withdrawing with a syringe (to avoid any oxidation of Co NCs), and solvent refluxing while heating. The solution was heated up to 140 °C with a heating rate of 10 °C $min^{-1}$, and then, more slowly, with a heating rate of 2 °C $min^{-1}$. After reaching 250 °C, the solution was maintained at this temperature for 60 min and then cooled under stirring to room temperature. Then, the solution was taken out of the flask using a syringe and placed in a tube under $N_2$ atmosphere, inside a glovebox. To avoid the aggregation of the NCs, a volume of dodecanoic acid (0.8 mL of $5 \times 10^{-3}$ M) was added. The next day, the solution was purified by suspension in (ethanol) and centrifugation (twice) to completely remove the (octylether) and the (dodecanoic acid) in excess. At the end, the NCs were dispersed in hexane (0.5 mL). The annealing treatment and all other steps took place under $N_2$ atmosphere.

## Acknowledgements

The authors would like to acknowledge the POSDRU/89/1.5/S/63663 and PNII-ID-PCCE-2011-2-0006 projects for financial support and to the collaboration under COST MP0904 Action.

Received: April 29, 2013
Published online: June 20, 2013

[1] G. Prieto, J. Zečević, H. Friedrich, K. P. de Jong, P. E. de Jongh, *Nat. Mater.* **2013**, *12*, 34–39.
[2] S. Sun, C. B. Murray, D. Weller, L. Folks, A. Moser, *Science* **2000**, *287*, 1989–1992.
[3] Y. Y. Liang, Y. G. Li, H. L. Wang, J. G. Zhou, J. Wang, T. Regier, H. J. Dai, *Nat. Mater.* **2011**, *10*, 780–786.
[4] V. F. Puntes, K. M. Krishnan, A. P. Alivisatos, *Appl. Phys. Lett.* **2001**, *78*, 2187–2189.
[5] C. T. Black, C. B. Murray, R. L. Sandstrom, S. H. Sun, *Science* **2000**, *290*, 1131–1134.
[6] K. M. Shaju, F. Jiao, A. Debart, P. G. Bruce, *Phys. Chem. Chem. Phys.* **2007**, *9*, 1837–1842.
[7] K. T. Lee, J. Cho, *Nano Today* **2011**, *6*, 28–41.
[8] K. Chokprasombat, *Walailak J. Sci. Technol.* **2011**, *8*, 87–96.
[9] M. P. Pileni, *J. Phys. Chem.* **2001**, *105*, 3358–3372.
[10] S. Singamaneni, V. N. Bliznyuk, C. Binek, E. Y. Tsymbal, *J. Mater. Chem.* **2011**, *21*, 16819–16845.
[11] K. J. Bishop, C. E. Wilmer, S. Soh, B. A. Grzybowski, *Small* **2009**, *5*, 1600–1630.
[12] E. V. Shevchenko, D. V. Talapin, N. A. Kotov, S. O'Brien, C. B. Murray, *Nature* **2006**, *439*, 55–59.
[13] M. A. Correa-Duarte, J. Pérez-Juste, A. Sánchez-Iglesias, M. Giersig, L. M. Liz-Marzán, *Angew. Chem. Int. Ed.* **2005**, *44*,4375–4378.
[14] Q. L. Zhang, S. Gupta, T. Emrick, T. P. Russell, *J. Am. Chem. Soc.* **2006**, *128*, 3898–3899.
[15] A. Tao, J. X. Huang, P. Yang, *Acc. Chem. Res.* **2008**, *41*, 1662–1673.
[16] V. Germain, M. P. Pileni, *Adv. Mater.* **2005**, *17*, 1424–1429.
[17] A. Taleb, F. Silly, A. O. Gusev, F. Charra, M. P. Pileni, *Adv. Mater.* **2000**, *12*, 633–637.
[18] V. Russier, C. Petit, J. Legrand, M. P. Pileni, *Phys. Rev. B* **2000**, *62*, 3910–3916.

[19] C. Petit, J. Legrand, V. Russier, M. P. Pileni, *J. Appl. Phys.* **2002**, *91*, 1502–1508.
[20] I. Lisiecki, D. Parker, C. Salzeman, M. P. Pileni, *Chem. Mater.* **2007**, *19*, 4030–4036.
[21] A. Taleb, C. Petit, M. P. Pileni, *J. Phys. Chem. B* **1998**, *102*, 2214–2220.
[22] P. Yang, H. Portalès, M. P. Pileni, *Phys. Rev. B* **2010**, *81*, 205405–205412.
[23] N. Zaitseva, Z. R. Dai, F. R. Leon, D. Krol, *J. Am. Chem. Soc.* **2005**, *127*, 10221–10226.
[24] J. V. Sanders, *Nature* **1964**, *204*, 1151–1153.
[25] A. Courty, A. Mermet, P. A. Albouy, E. Duval, M. P. Pileni, *Nat. Mater.* **2005**, *4*, 395–398.
[26] E. Duval, A. Mermet, A. Courty, P. A. Albouy, M. P. Pileni, *Phys. Rev. B* **2005**, *72*, 085439–085442.
[27] I. Lisiecki, V. Halte, C. Petit, M. P. Pileni, J. Y. Bigot, *Adv. Mater.* **2008**, *20*, 4176–4179.
[28] I. Lisiecki, M. Walls, D. Parker, M. P. Pileni, *Langmuir* **2008**, *24*, 4295–4299.
[29] I. Lisiecki, S. Turner, S. Bals, M. P. Pileni, G. Van Tendeloo, *Chem. Mater.* **2009**, *21*, 2335–2338.
[30] Z. Yang, I. Lisiecki, M. Walls, M. P. Pileni, *ACS Nano* **2013**, *7*, 1342–1350.
[31] D. Parker, I. Lisiecki, C. Salzemann, M. P. Pileni, *J. Phys. Chem. C* **2007**, *111*, 12632–12638.
[32] Y. Tang, M. Ouyang, *Nat. Mater.* **2007**, *6*, 754–759.
[33] D. Polli, I. Lisiecki, H. Portales, G. Cerullo, M. P. Pileni, *ACS Nano* **2011**, *5*, 5785–5791.
[34] S. Deville, E. Maire, G. Bernard-Granger, A. Lasalle, A. Bogner, C. Gauthier, J. Leloup, C. Guizard, *Nat. Mater.* **2009**, *8*, 966–972.
[35] J. Yang, J. Y. Ying, *Nat. Mater.* **2009**, *8*, 683–689.
[36] E. Klecha, D. Ingert, M. P. Pileni, *Langmuir* **2009**, *25*, 2824–2830.
[37] E. Klecha, D. Ingert, M. P. Pileni, *J. Phys. Chem. Lett.* **2010**, *1*, 1616–1622.
[38] Z. L. Wang, *J. Phys. Chem. B* **2000**, *104*, 1153–1175.
[39] A. H. Latham, M. E. Williams, *Langmuir* **2008**, *24*, 14195–14202.
[40] X. Y. Qi, Y. Z. Huang, M. Klapper, F. Boey, W. Huang, S. De Feyter, K. Mullen, H. Zhang, *J. Phys. Chem. C* **2010**, *114*, 13465–13470.
[41] J. W. Liu, J. Xu, Y. Ni, F. J. Fan, C. L. Zhang, S. H. Yu, *ACS Nano* **2012**, *6*, 4500–4507.
[42] C. Petit, P. Lixon, M. P. Pileni, *Langmuir* **1991**, *7*, 2620–2625.
[43] I. Lisiecki, M. P. Pileni, *Langmuir* **2003**, *19*, 9486–9489.
[44] M. Cavalier, M. Walls, I. Lisiecki, M. P. Pileni, *Langmuir* **2011**, *27*, 5014–5020.
[45] Z. Yang, M. Cavalier, M. Walls, P. Bonville, I. Lisiecki, M. P. Pileni, *J. Phys. Chem. C* **2012**, *116*, 15723–15730.
[46] M. Ishibashi, M. Itoh, H. Nishiraha, K. Aramaki, *Electrochim. Acta* **1996**, *41*, 241–248.
[47] I. Lisiecki, P. A. Albouy, M. P. Pileni, *Adv. Mater.* **2003**, *15*, 712–716.
[48] T. Pradeep, S. Mitra, A. S. Nair, R. Mukhopadhyay, *J. Phys. Chem. B* **2004**, *108*, 7012–7020.
[49] K. E. Mueggenburg, X. M. Lin, R. H. Goldsmith, H. M. Jaeger, *Nat. Mater.* **2007**, *6*, 656–660.
[50] Z. Qiao, J. Li, N. Zhao, C. Shi, P. Nash, *Scr. Mater.* **2006**, *54*, 225–229.
[51] S. C. Petitto, E. M. Marsh, G. A. Carson, M. A. Langell, *J. Mol. Catal. A: Chem.* **2008**, *281*, 49–58.